

# Physics 212 Final Project

Fall 2019

*Harvard University*

MAYA BURHANPURKAR AND ABIJITH KRISHNAN

## Contents

<b>1</b>	<b>Introduction</b>	<b>2</b>
1.1	Motivating Cosmological Inflation . . . . .	2
1.2	The Physics of Inflation . . . . .	2
1.2.1	Scalar Field Dynamics . . . . .	2
1.2.2	Physical Observations of Inflation Parameters . . . . .	3
<b>2</b>	<b>Computational Procedure</b>	<b>3</b>
<b>3</b>	<b>Results and Discussion</b>	<b>5</b>
<b>A</b>	<b>Guide to the Code</b>	<b>8</b>
A.1	Mukhanov Sasaki File . . . . .	8
A.1.1	Initialization . . . . .	8
A.1.2	Mukhanov-Sasaki Range . . . . .	8
A.1.3	Calculating Power Spectra . . . . .	9
A.2	Analysis File . . . . .	9
<b>B</b>	<b>Power Spectra</b>	<b>10</b>

# 1 Introduction

## 1.1 Motivating Cosmological Inflation

In the conventional Big Bang model of the universe, three problems arise from observations of cosmological parameters: the *flatness problem*, the *horizon problem*, and the *magnetic monopole problem*. These problems do not strictly contradict the conventional Big Bang model of the universe, but they require its initial conditions to be very finely tuned [2, 3].

The flatness problem is as follows: according to the equations of state of matter and radiation, any small deviation from a flat universe increases as the universe expands; i.e., a flat universe is a unstable fixed point. Current measurements of the sum of the density parameters,  $\Omega$ , indicate that our universe is flat to better than one part in 100. These equations of states thus imply that the curvature of the early universe must have been highly fine-tuned; i.e., the early universe must have been flat to one part in  $10^{60}$  under the conventional Big Bang model [2, 3].

The horizon problem of the universe is a consequence of the remarkable uniformity of the sky. For example, the Cosmic Microwave Background (CMB) is uniform to one part in  $10^5$ . However, under the conventional Big Bang model, only regions in the sky separated by at most 2 degrees could have been in causal contact with each other, and so the uniformity of the early universe must have been highly fine-tuned as well [2, 3].

Finally, the magnetic monopole problem arises due to predictions of current Grand Unified Theories (GUTs). GUTs predict that under spontaneous symmetry breaking of a single gauge theory, a large number of magnetic monopoles should arise. Under the conventional Big Bang model, the density of magnetic monopoles does not dilute enough during the expansion of the universe: we would expect to see many magnetic monopoles in our current universe, but we have not observed a single magnetic monopole [3].

Cosmological inflation, a theory of exponential expansion of space, offers a solution to these three problems outside of very specific fine-tuning of the early universe. During exponential growth of the scale factor  $a$ ,  $\Omega = 1$  is a stabled fixed point – thus resolving the flatness problem. Additionally, causal contact before this period of inflation established spatial homogeneity and resolves the horizon problem. Finally, an exponential growth of the scale factor after the GUT phase transition would dilute the density of magnetic monopoles sufficiently enough to account for the lack of observation of magnetic monopoles today. These resolutions and further observational data have supported the theory of cosmological inflation [2, 3].

## 1.2 The Physics of Inflation

### 1.2.1 Scalar Field Dynamics

The dynamics of inflation is often described by a single scalar field. Under the appropriate conditions, a single scalar field can result in an inflating universe by satisfying these three equivalent conditions:

$$\ddot{a} > 0, \quad \frac{d}{dt} \left( \frac{1}{aH} \right) < 0, \quad \rho + 3p < 0.$$

Here  $a$  is again the scale factor of the universe,  $H$  is Hubble's constant,  $\rho$  is the energy density of the universe and  $p$  is the pressure of the universe. The single scalar field is governed by the action

$$S = \int d^4x \sqrt{-g} \left[ \frac{1}{2}R + \frac{1}{2}g^{\mu\nu}\partial_\mu\phi\partial_\nu\phi - V(\phi) \right],$$

where  $g^{\mu\nu}$  is the metric,  $R$  is the Ricci scalar,  $(d^4x \sqrt{-g})$  is the volume form, and  $V$  is an inflationary potential. The resulting energy-momentum tensor for a Friedman-Robertson Walker metric and a homogenous scalar field is equivalent to the energy-momentum tensor of a perfect fluid with

$$\rho = \frac{1}{2}\dot{\phi}^2 + V(\phi), \quad p = \frac{1}{2}\dot{\phi}^2 - V(\phi).$$

Then, if  $V(\phi)$  is sufficiently larger than  $\dot{\phi}^2$ , the conditions of inflation will be met. While multiple potentials  $V(\phi)$  can result in inflation, not all potentials result in the inflationary parameters we observe today [2, 3].

### 1.2.2 Physical Observations of Inflation Parameters

Inflationary parameters are typically measured through the anisotropies and polarization data of the CMB. More specifically, these data give us the power spectra of the scalar and tensor modes of the CMB. Through the Mukhanov-Sasaki equation, we can obtain theoretical predictions of these power spectra for a given inflationary potential  $V(\phi)$ . Therefore, in this project, we build a Mukhanov-Sasaki solver that takes an inflationary potential as an input and outputs the power spectra for the scalar and tensor modes. We then compute power spectra for four inflationary potentials and compare our results to both the experimental data and theoretical predictions from the Planck collaboration [1].

## 2 Computational Procedure

We first evolve the scalar field  $\phi$  for the given inflationary potential  $V(\phi)$  until the end of inflation. Unless otherwise specified, our code will assume that we are in using natural units, i.e.,  $\hbar = c = M_{pl} = 1$ . The equation of motion for the scalar field  $\phi$  is given by

$$\ddot{\phi} + 3H\dot{\phi} + V_{,\phi} = 0, \quad 3H^2 = \frac{1}{2}\dot{\phi}^2 + V(\phi).$$

We can rewrite this second-order differential equation as a system of two first-order differential equations with an auxiliary variable  $\psi$ :

$$\psi = \dot{\phi}, \quad \dot{\psi} + 3H\psi + V_{,\phi} = 0, \quad 3H^2 = \frac{1}{2}\psi^2 + V(\phi).$$

Evolving these equations in terms of  $\log a$ , or the number of  $e$ -folds, instead of proper time  $t$  or conformal time  $\tau$ , is more numerically stable. We convert our differential equations using the relation

$$\frac{d}{dt} = \frac{da}{dt} \frac{d}{da} \frac{d}{d\log a} = \frac{\dot{a}}{a} \frac{d}{d\log a} \equiv H \frac{d}{d\log a}.$$

Once we make this change of variable, we obtain (using  $\frac{d}{d\log a}x = x'$ ) the following:

$$\psi = H\phi, \quad \psi' = -3\psi - V_{,\phi}/H, \quad 3H^2 = \frac{1}{2}\psi^2 + V(\phi).$$

Plugging the Friedmann equation (the last equation) into the two equations above gives us

$$\psi' = -3\psi - \frac{V'(\phi)}{\sqrt{\frac{1}{3}(\frac{1}{2}\psi^2 + V_{,\phi})}}, \quad (1)$$

$$\phi' = \frac{\psi}{H} = \frac{\psi}{\sqrt{\frac{1}{3}(\frac{1}{2}\psi^2 + V(\phi))}}. \quad (2)$$

Equations (1) and (2) can be numerically solved for  $\psi(\log a)$  and  $\phi(\log a) = \dot{\psi}(\log a)$ , given initial conditions for  $\phi_0$ ,  $\psi_0 = 0$ , and a range of  $\log a$  over which to evaluate. While we observed that our result was insensitive to our initial choice of  $\phi_0$ , we chose  $\phi_0 = 30$  for all potentials.

We then use our numerical results for  $\phi(\log a)$ ,  $\psi(\log a)$  and  $H(\log a)$  to solve the Mukhanov-Sasaki equation for both scalar and tensor perturbations. For scalar perturbations, the Mukhanov-Sasaki equation is given by

$$\overline{\overline{v}_k} + \left( k^2 - \frac{\bar{\bar{z}}}{z} \right) v_k = 0,$$

where  $v = z\mathcal{R}$ ,  $z = a\dot{\phi}/H = \bar{\phi}/H$ ,  $\mathcal{R}$  is the curvature perturbation, and  $\bar{f} = \frac{d}{d\tau}f$ . To convert conformal time derivatives to  $\log a$  derivatives, we use

$$\frac{d}{d\tau} = \frac{dt}{d\tau} \frac{d}{dt} = Ha \frac{d}{d\log a} = e^{\log a} H \frac{d}{d\log a} \quad (3)$$

Our strategy again is to write this as a system of first-order differential equations. If we substitute  $w_k \equiv \overline{v}_k$ , our differential equations are given by

$$w_k = e^{\log a} H v'_k \quad (4)$$

$$w'_k = \frac{-(k^2 - \bar{\bar{z}}/z)v_k}{e^{\log a} H}. \quad (5)$$

Here,  $\bar{\bar{z}}$  is given by

$$\bar{\bar{z}} = \frac{d}{d\tau} \left( e^{\log a} H z' \right) = e^{\log a} H (e^{\log a} H z')' = \frac{e^{2\log a} H z'}{z} \left( 1 + \frac{H'}{H} + \frac{z''}{z'} \right)$$

We can compute  $H$ ,  $H'$ ,  $z$ ,  $z'$ , and  $z''$  from the solution to the previous pair of differential equations and Friedmann equation. To solve for  $v_k$  and  $v'_k$  with (5), we use the Bunch Davies initial conditions: in the limit as  $\tau \rightarrow -\infty$ ,  $|k\tau| \gg 1$ , and so  $|k^2| \gg |\bar{\bar{z}}/z|$ . The resulting boundary conditions are

$$\lim_{\tau \rightarrow -\infty} v_k = \frac{e^{-ik\tau}}{\sqrt{2k}}.$$

With these initial conditions, if we plot the solutions,  $v_k$ , in the complex plane, they will travel in a circle around the origin until  $|k\tau| \approx 1$ , at which point the perturbations will exit the horizon.

Now consider tensor perturbations. The action is given by

$$S = \sum_{s=\{\times,+\}} \frac{1}{2} \int d\tau d^3k \left( (\overline{\overline{v}}_k^s)^2 - \left( k^2 - \frac{\bar{\bar{a}}}{a} \right) (v_k^s)^2 \right)$$

Computing

$$\frac{\partial \mathcal{L}}{\partial v_k^2} = -2v_k^s \left( k^2 - \frac{\bar{\bar{a}}}{a} \right), \quad \frac{d}{dt} \left( \frac{\partial \mathcal{L}}{\partial \overline{\overline{v}}_k^2} \right) = 2(v_k^s)^2$$

we apply the Euler-Lagrange equation to find

$$\overline{\overline{v}}_k^s = - \left( k^2 - \frac{\bar{\bar{a}}}{a} \right) v_k^s \quad (6)$$

Note that (6) has precisely the form as (3), and we repeat the same procedure to solve, writing

$$\begin{aligned}\bar{a} &= Ha \frac{da}{d \log a} = Ha^2 \\ \bar{\bar{a}} &= \overline{Ha^2} = Ha^3(H' + 2H)\end{aligned}$$

in terms of  $d \log a$ . We can additionally use the Bunch-Davies initial conditions for the tensor perturbation differential equation.

Now that we have computed the mode functions  $v_k$  for scalar perturbations and  $v_k^s$  for tensor perturbations, we compute the scalar and tensor power spectra. More specifically, we compute  $\Delta_{\mathcal{R}}^2(k) = \left(\frac{v_k H_*}{a \dot{\phi}_*}\right)^2$  and  $\Delta_h^2(k) = \left(\frac{2v_k^s}{M_{pl} a}\right)^2$ , where  $*$  indicates that we are computing these values at horizon crossing,  $k = aH$ .

With the scalar and tensor power spectra, we compute the spectral tilt,  $n_s$ , and the tensor-to-scalar ratio,  $r$ , for our potential  $V(\phi)$ . Given  $v_k$  and  $v_k^s$ , these are

$$n_s - 1 = \frac{d \log \Delta_s^2}{d \log k}, \quad (7)$$

$$r = \frac{\Delta_t^2(k)}{\Delta_s^2(k)} = \frac{2\Delta_h^2(k)}{\Delta_{\mathcal{R}}^2(k)}. \quad (8)$$

We place a guide to the code in Appendix Section A.

### 3 Results and Discussion

We ran our Mukhanov-Sasaki code for four potentials:

$$V_{2/3}(\phi) = \lambda_{2/3} \phi^{2/3}, \quad V_1(\phi) = \lambda_1 \phi, \quad V_{4/3}(\phi) = \lambda_{4/3} \phi^{4/3}, \quad V_2(\phi) = \lambda_2 \phi^2.$$

We set  $\lambda_{2/3} = \lambda_1 = \lambda_{4/3} = \lambda_2 = 0.1$  in our code. In Figure 1, we plot  $\phi(\log a)$  until the end of inflation, which occurs right before  $\phi = 0$ . All four plots have the same qualitative behavior apart from when inflation ends, which is dependent on the power law of  $V(\phi)$ . Table 1 lists the number of  $e$ -folds elapsed before the end of inflation.

$V(\phi)$	$e$ -folds Elapsed until end of inflation
$\phi^{2/3}$	676
$\phi$	450
$\phi^{4/3}$	338
$\phi^2$	225

Table 1: Number of  $e$ -folds elapsed until the end of inflation for  $V \propto \phi^{2/3}$ ,  $V \propto \phi^1$ ,  $V \propto \phi^{4/3}$ ,  $V \propto \phi^2$ .

With the scalar evolution equations numerically solved, we then computed  $v_k$  and  $v_k^s$  using the Mukhanov-Sasaki solver for the scalar and tensor perturbations respectively. To compare our

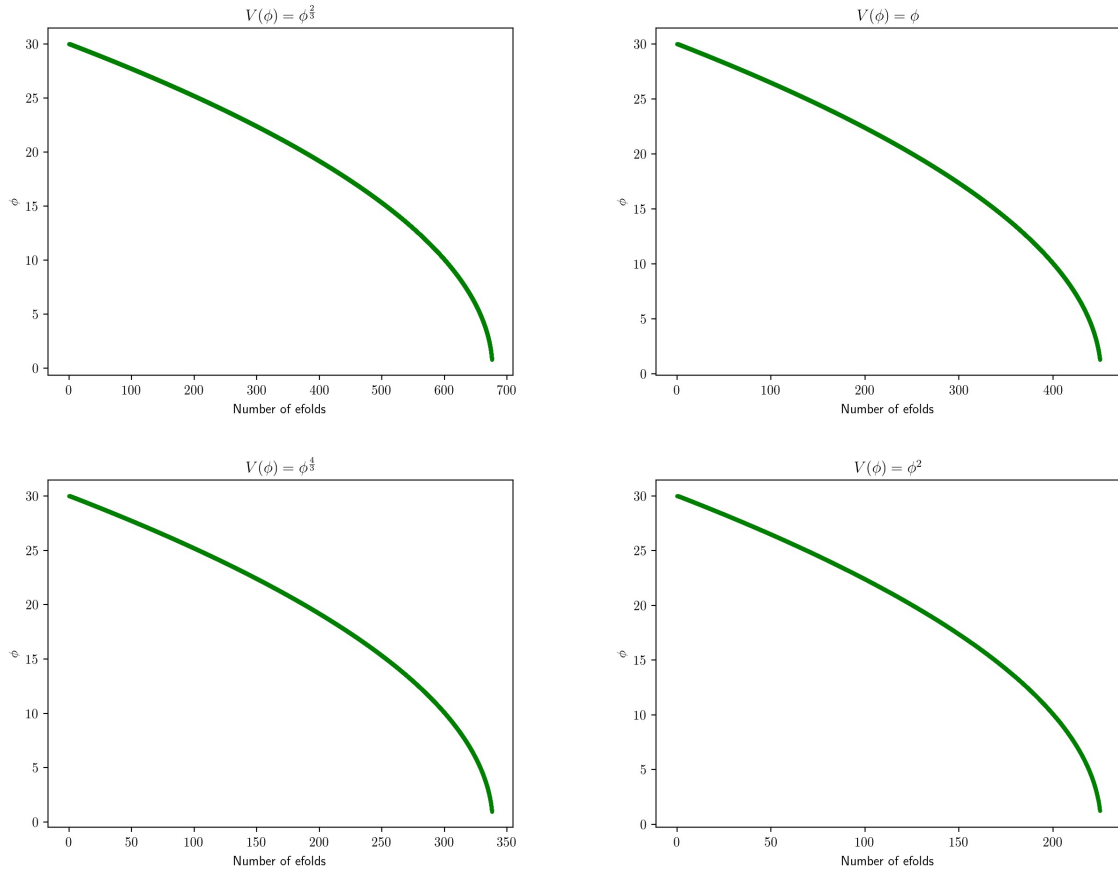


Figure 1: The evolution of the scalar  $\phi$  as a function of  $e$ -folds for  $V \propto \phi^{2/3}$ ,  $V \propto \phi^1$ ,  $V \propto \phi^{4/3}$ ,  $V \propto \phi^2$ .

results with the Planck paper, we computed  $v_k$  and  $v_k^*$  at  $N^* = 50$ , and  $N^* = 60$  respectively, where we computed  $v_k$  for the  $k$  modes that left the horizon roughly  $N^*$   $e$ -folds before the end of inflation [1]. Additionally, to give ourselves a physical scale equivalent to the one used in the Planck paper, we scale the  $k$ -mode that leaves the horizon  $N^*$   $e$ -folds before the end of inflation to  $0.05 \text{ Mpc}^{-1}$ . We plot the trajectory taken by  $v_k(\log a)$  in the complex plane in Figure 2.

From  $v_k$ , we compute the power spectra for scalar and tensor perturbations for all 4 potentials,  $N^* = 50$ , and  $N^* = 60$ . We sampled over 11  $k$ -values and  $\sim 2$  orders of magnitude of  $k$  for each plot. We place these plots in Appendix Section B. From these plots, we obtained the scalar tilt and the tensor-to-scalar ratio, located in Table 2. Additionally, in Figure 3, we overlaid our values of  $n_s$  and  $r$  with the experimental data in Figure 23 of the Planck paper [1].

As shown in the Table 2, the values we obtained for  $n_s$  were almost exactly the values the Planck collaboration obtained for  $n'_s$  [1] (apart from the  $V(\phi) \propto \phi^{2/3}$  and  $N^* = 50$  point). Therefore, our Mukhanov-Sasaki solver seems to be computing the scalar tilt properly. However, our  $r$  values were almost exactly a factor of 3 below the corresponding  $r'$  values. This discrepancy could be a result of a different convention that the Planck collaboration chose for the initial conditions of  $v_s^k$ . The Mukhanov-Sasaki equation is invariant under multiplying  $v_s^k$  by any multiplicative factor, so a different initial condition convention could result in the same qualitative behavior but different

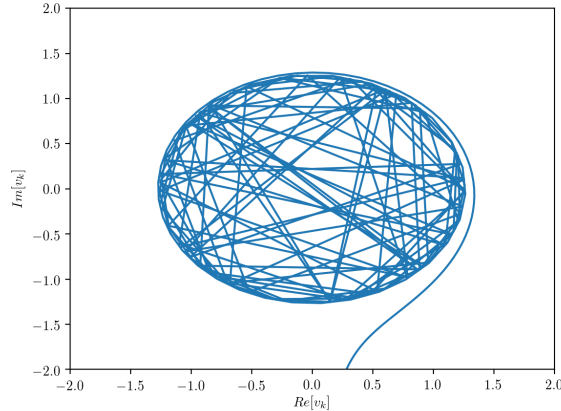


Figure 2: A parametric plot of  $v_k(\log a)$  in the complex plane. For this plot,  $k = 0.05 \text{ Mpc}^{-1}$ , after rescaling, and  $V(\phi) \propto \phi^{2/3}$ . We observe the expected behavior for  $v_k$ : an initially circular trajectory that eventually diverges in a straight line (at horizon crossing). Coarse sampling during the circular part of the trajectory resulted in lines that go through the interior of the circle.

50 e-folds	$\phi^{\frac{2}{3}}$	$\phi$	$\phi^{\frac{4}{3}}$	$\phi^2$	60 e-folds	$\phi^{\frac{2}{3}}$	$\phi$	$\phi^{\frac{4}{3}}$	$\phi^2$
$n_s$	.9798	.9702	.9699	.9623	$n_s$	.9776	.9755	.9726	.9666
$r$	.0180	.0261	.0350	.0509	$r$	.0148	.0217	.0290	.0424
$n'_s$	.9735	.9702	.9699	.9623	$n'_s$	.9776	.9752	.9724	.9671
$r'$	.0519	.0800	.1057	.1582	$r'$	.0442	.0669	.0878	.1319

Table 2: The  $n_s$  and  $r$  values we calculated, along with the  $n'_s$  and  $r'$  values found in the Planck paper. We estimated the  $n'_s$  and  $r'$  values from measuring the plot in the paper.

value of  $r$ . The discrepancy could also be a result of an oversight in how we computed  $\Delta_t^2(k)$  (which we discuss in detail in Appendix Section A). The plots of  $\Delta_t^2(k)$  do have a slightly nonzero tensor tilt (see Appendix Section B). Future work on this Mukhanov-Sasaki solver would aim to determine this discrepancy.

## References

- [1] Y. Akrami et al. Planck 2018 results. I. Overview and the cosmological legacy of Planck. 2018.
- [2] Daniel Baumann. Inflation. In *Physics of the large and the small, TASI 09, proceedings of the Theoretical Advanced Study Institute in Elementary Particle Physics, Boulder, Colorado, USA, 1-26 June 2009*, pages 523–686, 2011.
- [3] Cora Dvorkin. Lecture notes on cosmology, 2019.

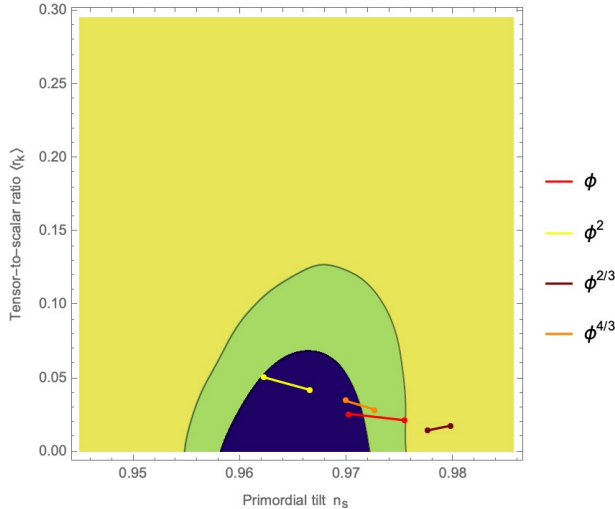


Figure 3: The  $n_s$  and  $r$  values we computed for the four given potentials, overlaid on top of the Planck experimental data. The left dot corresponds to  $N^* = 50$ , and the right dot corresponds to  $N^* = 60$  except for  $\phi^{2/3}$ .

## A Guide to the Code

### A.1 Mukhanov Sasaki File

In this section, we clarify some of the unintuitive choices we made in writing our Mukhanov-Sasaki code.

#### A.1.1 Initialization

We initialize our bounds of  $\log a$  such that inflation ends  $N^*$   $e$ -folds after  $\log a = 0$ . Determining the end of inflation, the parameter “efold” in the code, will take trial and error. We ran “model.get\_a\_phi()” and plotted  $\phi$  vs  $\log a$  to see at which  $e$ -fold inflation ended multiple times via binary search. Our results for when inflation ends for each potential are in Table 1. When we run the code to compute the power spectra, we change “efold” to match whichever potential we are using – this change is evident in the last few lines of our code.

#### A.1.2 Mukhanov-Sasaki Range

In lines 38-39 of the code, we ensure that we only solve the Mukhanov-Sasaki equation in the region  $\log a \in [-4 + \log k, 6 + \log k]$ . In other words, we are initializing  $v_k$  or  $v_k^s$  a few  $e$ -folds before horizon-crossing and solving the Mukhanov-Sasaki equation until a few  $e$ -folds after horizon-crossing. We made this choice solely because of numerical stability. If we initialized  $v_k$  or  $v_k^s$  at a time earlier than  $\log a = -4 + \log k$ , our code would be numerically unstable. We obtained the values  $-4$  and  $6$  from fine-tuning for a particular potential and  $k$ , but these values ended up working for all  $k$ , potentials, and  $N^*$  we tested. Additionally, our power spectra were insensitive to small changes in the bounds  $[-4 + \log k, 6 + \log k]$ .

### A.1.3 Calculating Power Spectra

In lines 123 and 168 of the code, we return the minimum of the  $\Delta_R^2$  and  $\Delta_t^2$  arrays instead of explicitly calculating the values of  $\Delta_R^2$  and  $\Delta_t^2$  at horizon crossing. With Figure 4, we can show why taking the minimum is a more appropriate measure of  $\Delta_R^2$ . As shown in the plot, the quantity

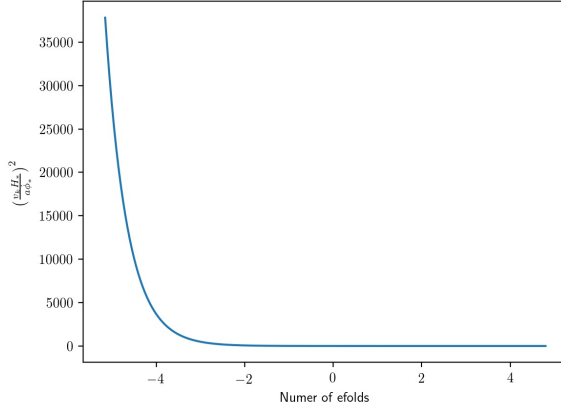


Figure 4: A plot of  $\left(\frac{v_k H}{a \dot{\phi}}\right)^2$  as a function of  $\log a$ . Here,  $k$  is chosen to be  $0.05 \text{ Mpc}^{-1}$  after rescaling. The plot was created for a  $V(\phi) \propto \phi^{2/3}$  potential. Horizon crossing occurs at  $\log a = 0$ .

$\left(\frac{v_k H}{a \dot{\phi}}\right)^2$  begins to converge to a fixed value at horizon crossing. However, after closer examination, the convergence happens slightly later than horizon crossing. Therefore, we obtain the values  $\Delta_R^2$  and  $\Delta_t^2$  converge to by taking the minimum of the arrays instead of taking their value at horizon crossing.

## A.2 Analysis File

After running “mukhanov\_sasaki.py”, we run ”analyse.py”. This analysis file is more straightforward apart from its command line inputs. The analysis file takes in 3 command line inputs: first the potential (’23’, ’1’, ’43’, or ’2’), then  $N^*$ , and then a quantity called “offset.” Offset allows us to rescale our  $k$  such that  $k = 0.05 \text{ Mpc}^{-1}$  crosses the horizon exactly  $N^*$  e-folds before the end of inflation.

To calculate “offset,” we ran “model.get\_a\_phi()” and computed the value of  $aH$  exactly  $N^*$  e-folds before the end of inflation. Note that the mode  $k$  crosses the horizon at  $aH$ . Then, by submitting the value of  $aH$  to “analyse.py” as the offset, we are submitting the  $k$  mode we are scaling to  $0.05 \text{ Mpc}^{-1}$ . In practice, because we initialize our code such that inflation occurs exactly  $N^*$  e-folds after  $\log a = 0$ , we compute  $H$  instead of  $aH$ . In Table 3, we provide values of  $H$  for various potentials, computed  $N^*$  e-folds before the end of inflation.

$V(\phi)$	$H(N^* = 50)$	$H(N^* = 60)$
$\phi^{2/3}$	0.316	0.316
$\phi^1$	1.003	1.050
$\phi^{4/3}$	1.076	1.126
$\phi^2$	4.495	4.920

Table 3:  $H$  computed exactly  $N^*$  e-folds before the end of inflation for various potentials.

## B Power Spectra

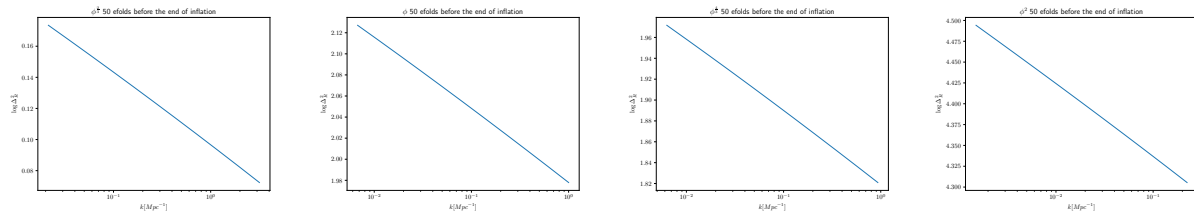


Figure 5: Scalar power spectra for inflation lasting for 50 efolds.

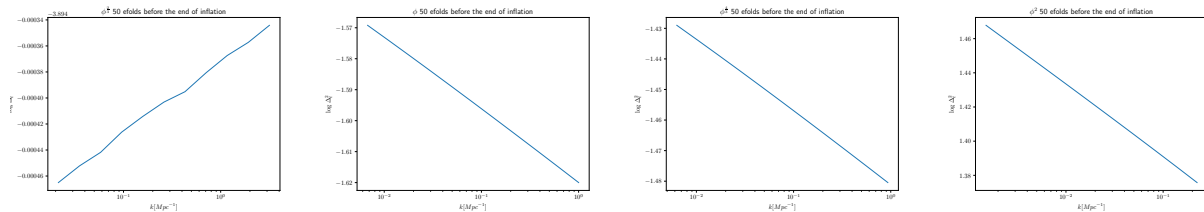


Figure 6: Tensor power spectra for inflation lasting for 50 efolds.

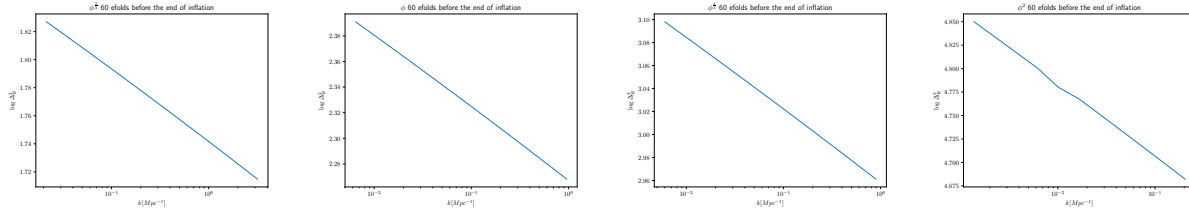


Figure 7: Scalar power spectra for inflation lasting for 60 efolds.

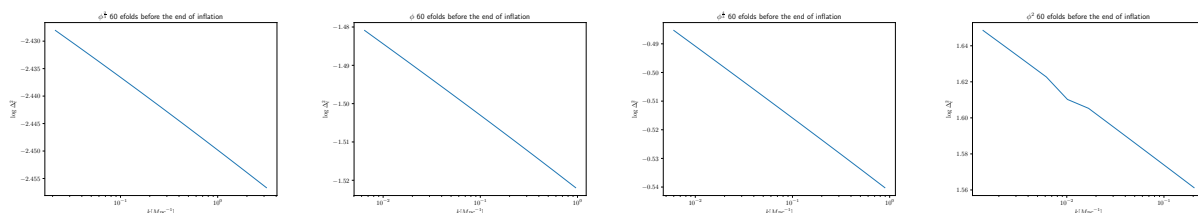


Figure 8: Tensor power spectra for inflation lasting for 60 efolds.